

PACS numbers: 42.55.Px; 42.60.Da; 42.60.Jf
DOI: 10.1070/QE2010v040n07ABEH014339

Catastrophic optical degradation of the output facet of high-power single-transverse-mode diode lasers. 2. Calculation of the spatial temperature distribution and threshold of the catastrophic optical degradation

D.R. Miftakhutdinov, A.P. Bogatov, A.E. Drakin

***Abstract*. The temperature distribution and the power threshold during the catastrophic optical degradation are calculated within the framework of the developed model of the COD of the output facet in high-power single-transverse-mode diode lasers. Comparison of the calculation results and the experiment show the model adequacy. The contribution of different physical mechanisms into the heating of the laser output facet is analysed. It is shown that the model under study can help to develop the method for predicting the laser lifetime by the accelerated ageing tests.**

Keywords: *high-power diode lasers, catastrophic optical degradation.*

1. Calculation technique

In the first part of the present work we have described the physical model for constructing the theory of catastrophic optical degradation (COD) [1]. In the second part, by using the developed model we have calculated the temperature distributions inside the laser resonator and the COD threshold for typical parameters of high-power single-transverse-mode near-IR (0.8 – 1.2 μm) lasers. The COD threshold involves such conditions under which there emerges spontaneous temporal avalanche-like temperature rise limited only by the irreversible damage of the laser material.

To determine these conditions, it is needed to calculate the temperature and intensity distributions of laser radiation inside the resonator. In our model [1], these distributions were found by using the self-consistent solution of one-dimensional (along the resonator axis z) laser problem with the distribution of carrier concentration $n(z)$ and output power $P^+(z)$ [$P^-(z)$] propagating in the positive (negative) direction of the z axis and by using the three-dimensional thermal problem with time dependent (in the general case) temperature distribution $T(x, y, z, t)$.

The optical flux power inside the resonator was found as the solution of the equation

$$\frac{\mathrm{d}P^{\pm}}{\mathrm{d}z} = \pm\left\{\Gamma\left[\sigma_0(\beta n(z) - \gamma n_0) - \alpha_0^{\mathrm{deg}} \exp\left(-\frac{z}{z_0}\right)\right] - \xi\alpha_0^{\mathrm{cl}} - \alpha_{\mathrm{int}}\right\} P^{\pm} \quad (1)$$

with the boundary conditions on the resonator mirrors

$$P^+(0) = R_1 P^-(0), \quad P^-(L) = R_2 P^+(L), \quad (2)$$

where R_1 and R_2 are the reflectivities of the front and rear mirrors, respectively. The carrier concentration n, entering (1), was determined by the expression

$$n = n_0\left[\left(\frac{j}{j_0}\right)\phi(z) + \gamma\left(\frac{P^+ + P^-}{P_{\mathrm{sat}}}\right)\right] \times \left[1 + \eta + \frac{Q\tau}{\lambda}\exp\left(-\frac{z}{\lambda}\right) + \beta\left(\frac{P^+ + P^-}{P_{\mathrm{sat}}}\right)\right]^{-1}, \quad (3)$$

which includes the current density j_0 required to achieve the medium transparency and the saturation power P_{sat}:

$$j_0 = \frac{n_0 e d}{\tau}, \quad P_{\mathrm{sat}} = \frac{\hbar\omega d w}{\sigma_0 \Gamma \tau}. \quad (4)$$

The parameters entering equations (1) – (4), such as the optical confinement factor Γ, stimulated transition cross section σ_0, medium transparency density n_0, surface recombination rate Q, carrier lifetime τ, function $\phi(z)$ describing diffusion spreading of carrier concentrations in the case of current limitation, carrier diffusion length λ, losses in cladding layers α_0^{cl} and degraded layer α_0^{deg}, are determined in paper [1]. Additionally to above-described losses, equation (1) includes losses α_{int} caused by the optical inhomogeneities of the medium, which lead to laser radiation scattering and make no direct contribution into the local heat release. They result only in the general heating of the laser diode and are neglected as thermal sources within the framework of our model. Typical values of all the parameters used in calculations are listed in Table 1. Equations (1) and (3) are the result of integration of the equations for the laser radiation intensity and active carriers over the cross section in the xy plane. They are also the balance equations for the energy and particles in the thin layer lying in the xy plane passing through point z. As a result of this averaging over the xy plane, there appear dimensionless parameters β, γ, ξ, η of the order of unity, which take into account the spatial overlap of the temper-

D.R. Miftakhutdinov, A.P. Bogatov, A.E. Drakin P.N. Lebedev Physics Institute, Russian Academy of Sciences, Leninsky prosp. 53, 119991 Moscow, Russia; e-mail: mifta@sci.lebedev.ru

Received 26 April 2010
Kvantovaya Elektronika **40** (7) 589 – 595 (2010)
Translated by I.A. Ulitkin

Table 1.

Notation	Physical quantity	Basic value
C_1	Heat capacity of cladding layers	1.84 J cm^{-3} K^{-1}
C_2	Heat capacity of the output facet coating	1.79 J cm^{-3} K^{-1}
$\tilde{T}$	Surrounding temperature	300 K
κ_1	Heat conductivity of cladding layers	0.15 W K^{-1} cm^{-1} (for $T = \tilde{T}$)
κ_2	Heat conductivity of the output facet coating	0.14 W K^{-1} cm^{-1} (for $T = \tilde{T}$)
n_κ	Dimensionless coefficient	1.3 (for $T = \tilde{T}$)
$\partial n_\kappa/\partial T$		-5.4×10^{-4} K^{-1}
d	Active region thickness	90 Å
w	Active region width	5 μm
λ	Carrier diffusion length in the direction of the z axis	1.5 μm
V_{p-n}	Voltage at the p – n transition	1.5 V
$\hbar\omega$	Photon energy of laser radiation	1.265 eV
E_a^g	Bandgap width in the active region	1.265 эВ ($E_a^g = \hbar\omega$) (for $T = \tilde{T}$)
$\partial E_a^g/\partial T$		-0.0005 eV K^{-1}
τ	Time of spontaneous emission	1 ns
T_b	Temperature at which $\tau = \tau_{nr}$	450 K
T_{nr}	Characteristic temperature of nonradiative recombination increase	150 K
α_0^{deg}	α^{deg} at the crystal boundary	20000 cm^{-1}
z_0	Depth of the degraded region	0.5 μm
Q	Surface recombination coefficient	1.5×10^5 cm s^{-1}
α_0^{cl}	Absorption in cladding layers at $\hbar\omega = E_{eff}$	8000 cm^{-1}
E_{eff}^0	Effective energy of intraband transition in cladding layers at $T = 0$	2 eV
k	Boltzmann constant	8.6×10^{-5} eV K^{-1}
θ_E	Einstein temperature	260 K
p	Dimensionless coupling constants	0.09
q		6
Λ	Disorder parameter	5
x_0	Characteristic dimensions of the intensity distribution along the x axis	0.24 μm
x_s		1.225 μm
h	Exponent	1.62
A	Normalisation coefficient for $u(x)$	5.64 μm^{-1}
Γ	Optical confinement factor	0.0155
y_s	Characteristic dimensions of the intensity distribution along the y axis	3 μm
σ	Differential gain	5×10^{-16} cm^2 (for $T = \tilde{T}$)
n_0	Density at which transparency is achieved	1.5×10^{18} cm^{-3} (for $T = \tilde{T}$)
T_σ	Characteristic temperature of the differential gain	200 K
T_N	Characteristic temperature of the transparency density	90 K
T_0	Characteristic temperature of the current threshold	164 K
L	Laser length	0.1 cm
α_{int}	Scattering losses in the laser resonator	5 cm^{-1}
R_1 (R_2)	Reflectivity with respect to the power from the front (rear) mirror	0.05 (0.95)

ature field with the spatial intensity distribution of the optical flux and with the spatial inversion distribution:

$$\beta(z) = \frac{1}{y_s}\int \exp\left[-\frac{\pi y^2}{W^2} - \frac{T(0,y,z) - \tilde{T}}{T_\sigma}\right]dy,$$

$$\gamma(z) = \frac{1}{y_s}\int \exp\left[-\frac{\pi y^2}{y_s^2} - \frac{T(0,y,z) - \tilde{T}}{T_0}\right]dy,$$

$$\xi(z) = A y_s^{-1}\int\left[1 + \left(\frac{x}{x_0}\right)^h\right]^{-1} \exp\left[-\pi\left(\frac{x^2}{x_s^2} + \frac{y^2}{y_s^2}\right)\right.$$

$$\left. + \frac{\hbar\omega - E_{eff}^0 + pk\theta_E \exp[\theta_E/T(x,y,z) - 1]^{-1}}{qk\theta_E[(1+\Lambda)/2] + \exp[\theta_E/T(x,y,z) - 1]^{-1}}\right]dx dy, \quad (5)$$

$$\eta(z) = \frac{1}{w}\int \exp\left[-\frac{\pi y^2}{w^2} + \frac{T(0,y,z) - T_b}{T_{nr}}\right]dy,$$

where $W = (w^{-2} + y_s^{-2})^{-2}$, other parameters being determined in [1].

The stationary equation for the temperature field $T(x,y,z)$ has the form

$$\mathrm{div}[\kappa(x,y,z,T)\mathrm{grad}T] + F(x,y,z,T) = 0, \quad (6)$$

where the function of the thermal sources $F(x,y,z,T)$ is found in [1]; all the quantities entering into it and specified by $n(z)$ and $P^{\pm}(z)$ are determined by equalities (4), (5) and the laser parameters presented in Table 1. Because the active region thickness d of the laser is, as a rule, much smaller than all the characteristic dimensions of both the thermal and laser problems, the sources of the heat released in the active region in numerical calculations are replaced by the corresponding thermal fluxes from the infinitely thin layer. In this case, equation (6) can be solved only for two functions of the heat conductivity coefficient: $\kappa_1(T)$ for the heat conductivity of cladding layers and $\kappa_2(T)$ for the heat conductivity of the material deposited on the facet. In solving the thermal problem, we used the following boundary conditions: the end facets are thermally insulated, the temperature of the side facets is equal to the surrounding temperature.

The algorithm of numerical calculations is based on the scheme presented in Fig. 1. This scheme takes into account the fact that the characteristic time needed to establish the stationary intensity distribution inside the laser resonator is many orders of magnitude smaller than the characteristic time needed to establish the stationary temperature distribution. The basic parameter in finding the solution for $T(x,y,z)$, $P^{\pm}(z)$, and $n(z)$ is the laser pump current J changing in the region $J_0 < J < J_{cr}$. Here, J_{cr} is the maximum current at which the stationary solution still exists. The current J_{cr} together with the power P_{cr} corresponding to it (hereafter, the subscript 'cr' is used for all physical quantities characterising the solution of the stationary problem for the pump current J_{cr}) are the threshold COD values for the pump current and the laser power. Mathematically, the breakdown point of the stationary solution can be characterised by point J_{cr}, the derivative $\partial T/\partial J$ increasing infinitely when tending to this point. In numerical calculations with the finite step over the current ΔJ, calculations will obviously terminate at J, which differs

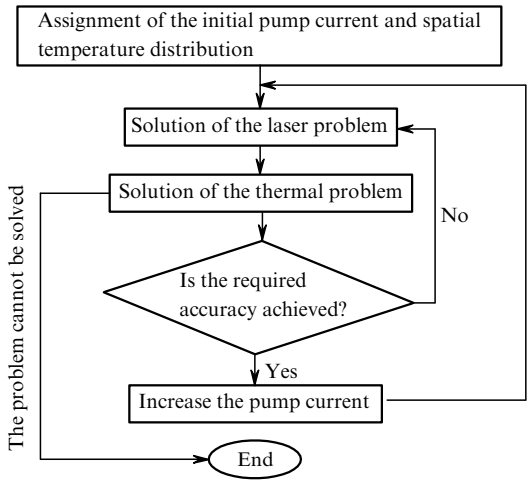

Figure 1. Algorithm of solution of the stationary problem.

from J_{cr} by ΔJ. This value determines the accuracy of finding the COD threshold within the accepted model.

We studied the dynamic characteristics of the COD by solving the nonstationary heat conduction equation

$$\mathrm{div}[\kappa(x,y,z,T)\mathrm{grad}T] + F(x,y,z,T) = C\frac{\mathrm{d}T}{\mathrm{d}t}, \qquad (7)$$

the algorithm of its solution being somewhat different. We took into account the fact that the volume of the heated region near the output mirror is rather small compared to the total resonator volume, and thus does not affect the laser power. This is confirmed below by the calculation results for the stationary case. Therefore, we can assume with a higher degree of accuracy that the COD develops when the laser power and carrier distribution in the resonator volume do not change in time. Equation (7) [namely, the function of thermal sources $F(x,y,z,T)$] includes two parameters determined by the solution of the laser problem [carrier concentration $n(z)$ and optical power $P^{\pm}(z)$] and the pump current J. To solve the equation, we used the following values of these parameters:

$$n(z) = n_{cr}(z), \quad P^{\pm}(z) = P^{\pm}_{cr}(z)K, \quad J = J_{cr}K, \qquad (8)$$

where the coefficient $K > 1$.

All calculations were performed on a personal computer (Intel Core 2 Duo 2.2 GHz). Calculations of the dependence of the temperature profile on the pump current, resulting in finding the COD threshold for one set of the parameters, took on average an hour. The thermal problem both in the stationary and nonstationary cases was solved with the help of FlexPDE (www.pdesolutions.com).

2. Results of numerical calculations and their discussion

Figure 2 and 3 present the results of the solution of the self-consistent stationary problem for a basic set of the parameters. It follows from Fig. 2 that at given $z_0 =$ 5 μm, the lasing efficiency is 0.92 W A^{-1} and the threshold current is 43 mA, which coincides with a greater accuracy with the corresponding values that can be found analytically by using the distributed loss approximation and data from Table 1. The size z_0 of the degraded region near the output mirror weakly affects the output parameters of the laser. This is clearly demonstrated by the data in Fig. 3, which can help to determine the decrease in the output power of the laser at a constant (working) laser current with increasing the optical losses due to an increase in z_0. The quantity $P^{-1}(\partial P/\partial z_0)$ in this case is $\sim 3 \times 10^{-2}$ μm^{-1}.

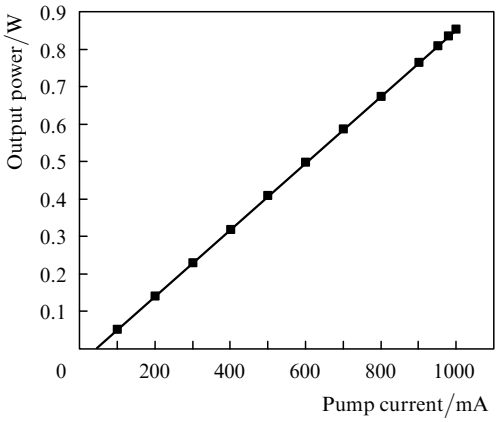

Figure 2. Light–current characteristic for a basic set of parameters.

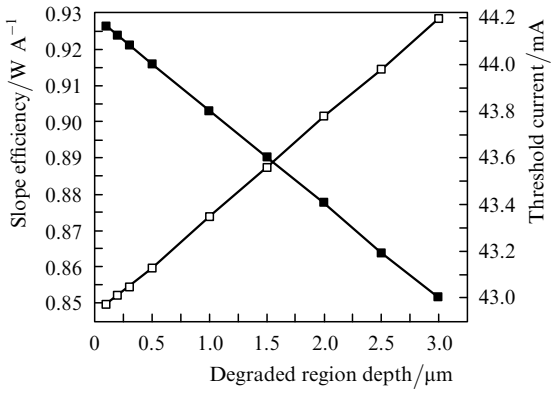

Figure 3. Dependences of the slope efficiency (■) and threshold current (□) on the depth of the degraded region.

On the contrary, the temperature and, accordingly, P_{cr} strongly depend on z_0. Figure 4 shows the temperature dependences of the pump current at the surface centre of the laser output facet ($x = y = 0$) with respect to the surrounding temperature (i.e., $T - \tilde{T}$). The dependence $T - \tilde{T} = f(J)$, in accordance with the data of Figs 2 and 3, can be presented as the temperature dependence of the laser output power P. The upper scale illustrates this dependence (note that because the efficiency and the threshold current weakly change with z_0, we can use for this dependence the same power scale for all z_0). The parameter of the curves is z_0. One can see that at the initial segment the dependence $T - \tilde{T} = f(P)$ is close to linear. The slope coefficient $\partial T/\partial P$ for $\alpha_0^{deg} = 2 \times 10^4$ cm^{-1} and z_0 lying in the range 0.1–3 μm varies from 80 to 670 K W^{-1}, which will correspond to the data from papers [2–6], if we normalise their values to the values of the parameters used in calculations. With increasing the laser output power, the slope of the curves invariably increases (it is also well seen in the experiments [4, 6]) and at $P = P_{cr}$ the stationary solutions breaks down. A decrease in the step over the current J in numerical calculations within

the accepted accuracy does not change the situation. Analysing the data of Fig. 4, we can pay attention to the fact that the higher P_{cr}, the sharper the passage to the breakdown (i.e., at a fixed step over the current, smaller values of $\partial T/\partial J$ at point preceding the breakdown correspond to larger values of P_{cr}). This fully characterises the qualitative representation (described in [1]) of the COD development as the process with the positive feedback. The calculation region P_{cr} satisfactorily agrees with the experimental data of papers [7–12]. Of course, one should take into account some freedom in the choice of z_0 and α_0^{deg}, which was mentioned above and in the first part of the present work [1]. According to data, for example, of papers [4, 13], depending on the manufacturing technology and the operating conditions the parameters z_0 can be in the range from submicrons to several microns.

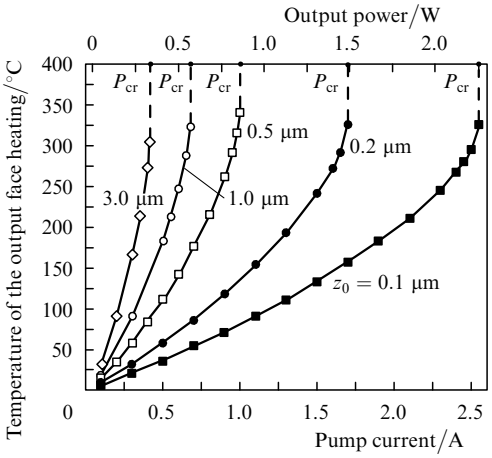

Figure 4. Dependences of the temperature of the output facet heating with respect to the surrounding temperature $T - \tilde{T}$ on the pump current (output power) for different depths z_0 of the degraded region.

Processing of the data similar to those presented in Fig. 4 makes it possible to find the dependence of the threshold power of the COD on the depth of the degraded region z_0. This dependence shown in Fig. 5 for a basic set of the parameters can be of great importance not only for determining the maximally achievable output power of the laser but also for predicting its reliability and lifetime. Indeed, as was noted in [1], the depth z_0 increases with the laser lifetime and the range of this increase is determined by the formation rates of defects and their diffusion near the laser output facet. Of course, we should understand that finding the dependence of z_0 on the laser lifetime is the solution of a quite different problem related to the material degradation and defect formation at high temperatures, optical flux intensities, and nonradiative recombination rates. But if we can estimate somehow this dependence, by using the data similar to those presented in Fig. 5 we can assess the maximum laser lifetime. For the given working level of the laser output power P, it will mean that P_{cr} will decrease down to P by the end of the operation time t_{lim}, i.e., $P_{cr}(t_{lim}) = P$, which is shown in Fig. 5 by a dashed line. If we assume that the defects diffuse along the z axis with a constant velocity D, then $z_0^2(t) = z_0^2(0) + Dt$. The time t in arbitrary units (thousands of hours in the example considered below), corresponding to the values of z_0, is shown near each point on the curve in Fig. 5.

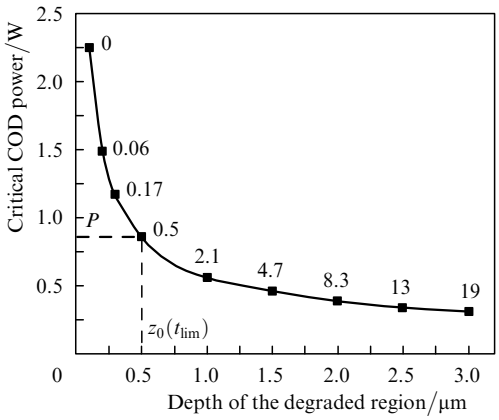

Figure 5. Dependences of the critical COD power on the depth of the degraded region [near the points is shown the limiting operation time t_{lim} (in arbitrary units) under assumption of the constant coefficient of the defect diffusion along the z axis].

It is pertinent to note that within the framework of the present theory, calculations involving the data of Figs 3 and 5 make it possible to determine simultaneously a decrease in P_{cr} and the working output power of the laser with increasing z_0. This drastically limits the range of best-fit values α_0^{deg} and z_0 from the experiments and thus increases the reliability of the predictions of the laser lifetime. Because the slope efficiency of the laser is determined by the ratio of the losses at the output mirror to the total losses, we can easily obtain that

$$\Gamma\Delta(\alpha_0^{deg} z_0) = \left|\frac{\Delta P}{P}\right| \alpha_{tot} L, \tag{9}$$

where α_{tot} are the total mode losses including mirror losses but neglecting the losses caused by degradation; $\Delta P/P$ is the relative change in the power during the laser lifetime. The rate of a decrease in the laser output power experimentally obtained in paper [11], which is $2 \times 10^{-6} - 2 \times 10^{-5}$ h^{-1}, corresponds to $\Delta(\alpha_0^{deg} z_0)$ in the range 0.1–1 for the operation time of 500 h. At $P_{cr} = 850$ mW and the rate of the output power drop 2×10^{-5} h^{-1}, we obtain that after 500 h of operation, $\alpha_0^{deg} = 2 \times 10^4$ cm^{-1} and $z_0 = 0.5$ μm, while the rate of defect diffusion is $D = 0.5$ μm$^2 \times 10^{-3}$h^{-1}. The time t_{lim} shown in Fig. 5 corresponds to these parameters.

Figure 6 presents the temperature distribution along the resonator axis on a segment near the output facet of the laser diode. The point $z = 0$ corresponds to the interface between the materials of the active region and the coating of the output dielectric mirror. The parameter of the curves is the pump current of the laser and its corresponding values of the output power. One can see that the region with the maximal temperature is located not at point $z = 0$ but shifted approximately by 1 μm inside the laser diode resonator due to the additional heat removal from the overheated region, ensured by the coating of the laser output facet.

The transverse temperature distributions for the optical power near P_{cr} and different cross sections $z = \text{const}$ are shown in Fig. 7. One can see that the cross section area of the overheated region is rather small (~ 3 μm^2) (Fig. 7c) and its volume, taking into account the data of Fig. 6, is ~ 3 μm^3. The calculated data agree with the results of

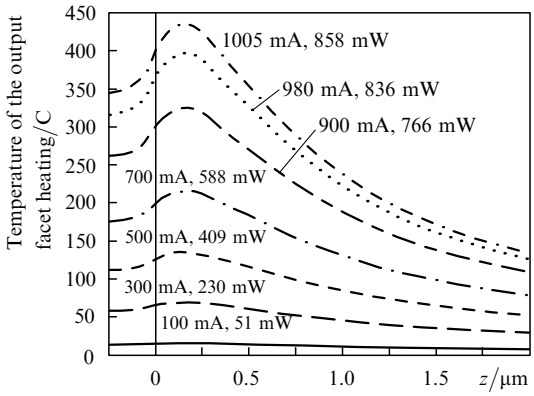

Figure 6. Heating temperature distribution $T - \tilde{T}$ along the z axis at different pump currents and output powers of the laser.

the experiments performed in papers [7–9]. Because the characteristic dimensions of thermal sources along the x axis are markedly smaller than those along the y axis, the overheated region cross section has an almond-like shape extended along the y axis, this region being most strongly elongated at the point corresponding to the region with a maximal temperature (Fig. 7c). The shape of the damaged surface of the output mirror observed in the experiments [7–9] fully confirm these results.

The dependence of the critical COD power P_{cr} on the action of different physical mechanisms is illustrated in Figs 8–11, which makes it possible to evaluate the conditions under which these mechanisms begin to work and even dominate. Thus it follows from Fig. 8 that at the surface recombination rate $Q > 3 \times 10^4$ cm s^{-1}, P_{cr} starts noticeably decreasing. These data allow one to formulate the necessary requirements to the surface quality of the laser facet in terms of the surface recombination so that it could not significantly affect the COD threshold. The influence of the volume nonradiative recombination on the COD threshold can be assessed from the data of Fig. 9. They indicate that it decreases substantially only at a rather strong temperature dependence of the recombination when the characteristic temperature is $T_{nr} < 100$ K.

The data of Fig. 10 allow one to analyse the increase in the COD threshold due to an additional heat removal ensured by the coating of the diode output facet, which

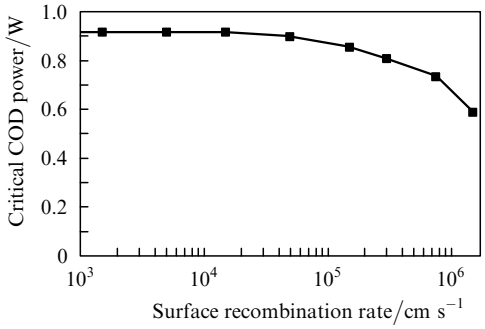

Figure 8. Dependence of the critical COD power on the surface recombination rate.

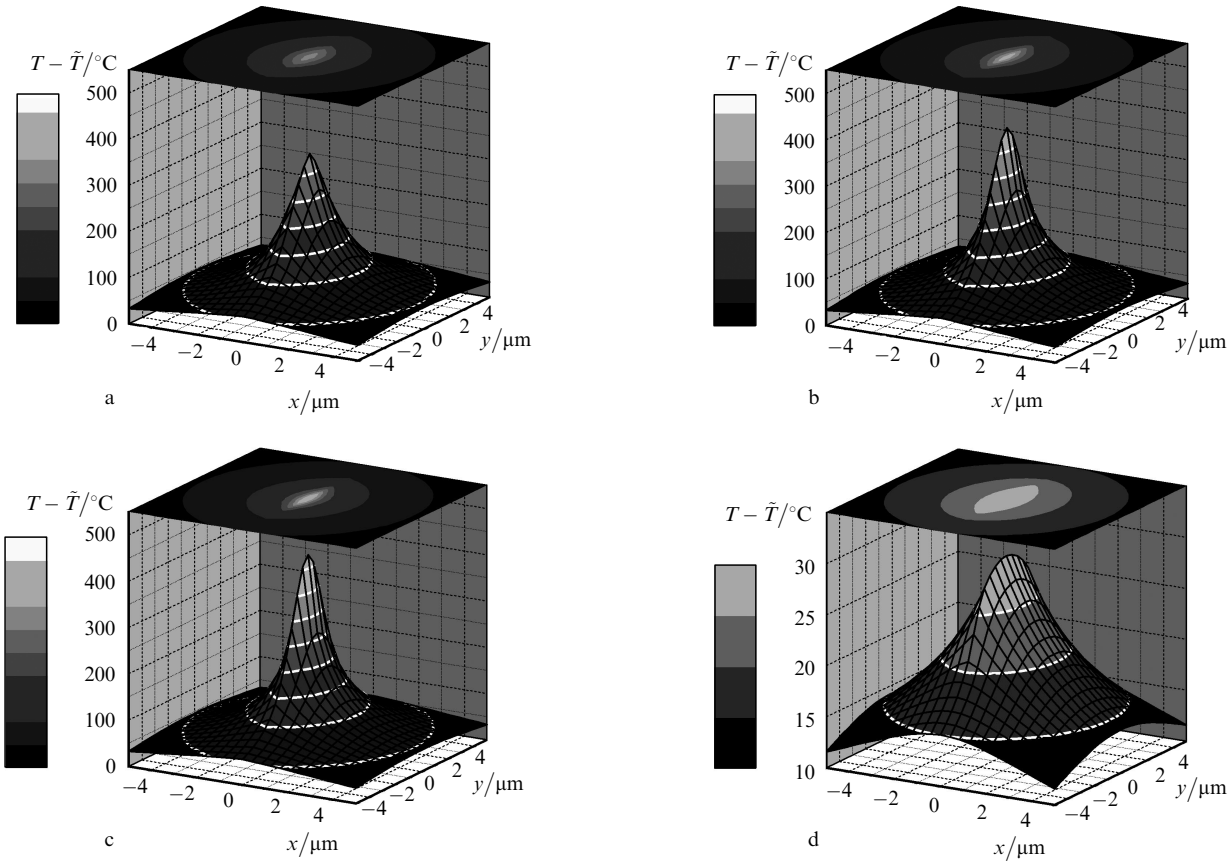

Figure 7. Heating temperature distribution $T - \tilde{T}$ in the plane xy on the surface of the protective coating (a), at the interface between the output mirror and the protective coating (b), in the region of the maximal temperature (c), and within the volume of the laser (d).

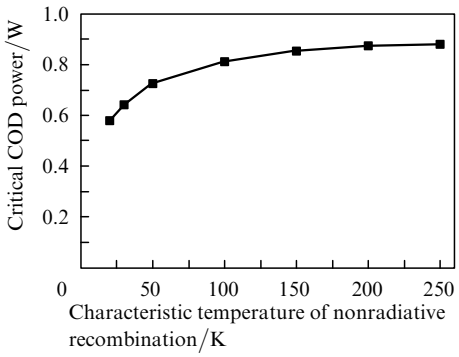

Figure 9. Dependence of the critical COD power on the characteristic temperature of nonradiative recombination.

makes it possible to optimise the total length of the output facet coating. Indeed, in some specific case corresponding to Fig. 10, the optimal thickness of the coating is ~ 1.5 μm. When the coating is thicker, the COD threshold stops increasing while the probability of the exfoliation of a 'thick' coating from the diode facet can increase.

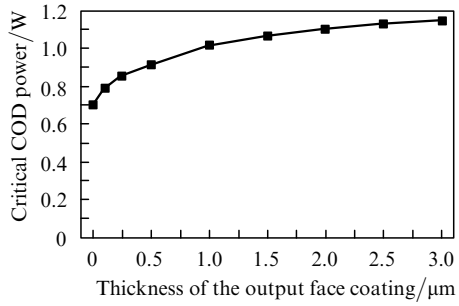

Figure 10. Dependence of the critical COD power on the thickness of the protective coating of the output facet.

The residual absorption in wide-band layers caused by the violation of the crystallographic order affects the COD threshold only when the disorder parameter is $\Lambda > 60$ (Fig. 11). Figure 11 also presents the values of the optical absorption corresponding to the maximal temperature at the point close to the COD threshold.

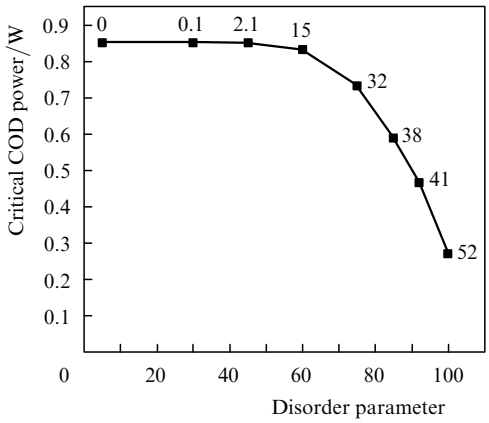

Figure 11. Dependence of the critical COD power on the disorder parameter Λ. Digits at the points are the values of the optical absorption (in cm^{-1}).

The calculations also showed that the optical density of the near-surface (degraded) layer, i.e., the product $\alpha_0^{deg} z_0$, does not serve as an invariant when determining both the threshold and the temperature dependence of the pump current even under the conditions $\alpha_0^{deg} z_0 \ll 1$. It turned out that P_{cr} starts drastically decreasing with increasing α_0^{deg} rather than z_0.

Investigation of the COD dynamics revealed a substantial feature consisting in the fact that the COD is preceded by rather long heating time of the destruction region adjacent to the region of a markedly larger volume. Because of this the COD development time has a rather 'inertial' component, which is illustrated in Fig. 12. The direct optical damage of the facet starts at temperatures above 1200 °C. As follows from Fig. 12, in the used temperature and time scales the dependences $T_{max}(t)$ have almost a vertical slope. The calculations showed that in this segment the rate of change in the temperature exceeds 40 K ns^{-1}, in agreement with the experimental data according to which a decrease in the laser power during the COD occurs within 50–80 ns. The segment of a drastic temperature rise is preceded by the segment of its relatively slow rise. The duration of this segment depends on the pump current and can be greater than 10 μs when the output power exceeds P_{cr} by no more than 10 %.

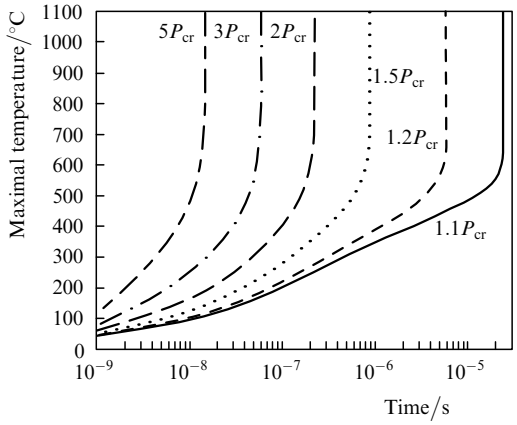

Figure 12. Time dependences of the maximal temperature in the laser resonator for different excess of the output power over the threshold COD power.

These data indicate that in the pulsed excitation regime, the COD threshold can be increased if during the pulse action the process does not have time to pass the slow segment of its development. However, the possibilities of this increase are limited. In this particular case, when the critical values for the stationary regime exceeds three-fold the pulsed output power, the duration of the slow segment decreases down to ~ 50 ns, i.e., down to those values which characterise the irreversible COD process itself [7–9].

The calculations also showed that blocking the current on a segment of thickness a in the region of the output facet does not lead to a noticeable increase in the COD threshold. Thus, at $a = 10$ μm, P_{cr} increases approximately by 10 %, and at $a < 10$ μm, P_{cr} does not change due to the carrier diffusion or due to the current spreading. At $a > 10$ μm, P_{cr} also remains almost the same because the carrier concentration on this segment at a large laser power is determined by the optical absorption rather than by the pump current.

The above results were obtained for well-defined parameters of the active medium, heterostructure layers, and laser resonator. As was already noted in [11], most of these values are not physical constants but rather the data characterising the state of the laser medium both after some different technological processes during the laser fabrication and after some period of its operation. Therefore, the parameters used in calculations (see data of Table 1) in principle cannot have strictly identical values even for lasers of the same design, which are manufactured using close technologies as well as some uniform COD threshold cannot be realised for such lasers in practice. This circumstance is the basic reason behind a significant scatter in the values of P_{cr} and J_{cr} for different samples of the laser diodes. Another matter is that to define correctly the results, we used basic values of these parameters corresponding, to the highest degree, to the state-of-the-art of the technology and production of the most wide-spread lasers whose design makes it possible to compare adequately the results of calculations and experiments.

3. Conclusions

The both parts of the present work are devoted to the development of the COD theory as applied to modern high-power diode lasers. The theory is based on the optical absorption by a defect layer, which is some initial (seed) mechanism triggering the COD. The calculations of the temperature distribution in the laser resonator volume, the values of P_{cr}, and other laser parameters satisfactorily agree with the experiment, which counts in favour of the adequacy of the theory.

The theory allows one to formulate the requirements to the optical quality of the laser medium and the output facet in order to provide the reliable operation of the laser. Thus, we have shown that at the given laser parameters, the surface recombination rate Q should not exceed 10^5 cm s^{-1} so that not to limit the laser reliability and the output power, while the temperature growth rate of the volume non-radiative recombination should be characterised by the parameter $T_{nr} > 100$ K so that not to affect significantly the threshold COD power. In addition, the crystallographic perfection of the emitters (cladding layers) should be such that, when heated by 400 °C, absorption in them at the laser wavelength is less than 10 cm^{-1}.

Besides, using the calculations it is possible to establish the relation between the character of the dependence of the temperature at the laser output mirror on the laser power and the rate of decrease in P_{cr} as well as between the 'slow' decrease in the laser output power and the period of the laser operation and lifetime. This, in total, opens new possibilities of creating new methods for determining the lifetime of the lasers (produced with the help some specific technology) by using some accelerated ageing tests.

Finally, the revealed strong dependence of P_{cr} on the thickness of the degraded damaged layer makes it possible to search for the ways of increasing the radiation resistance of the laser output facet and thus of increasing the laser lifetime and output power. Note here the importance of passivation of the diode output facet cleavage, which would provide the minimal values of the parameters α_0^{deg} and z_0.

Note in conclusion that in this paper we have treated the COD as the damage of the diode output facet. Nevertheless, using the obtained results we can suggest that under certain conditions, for example, in the presence of a defect segment in the active region with a sufficient absorption α_0^{deg} and thickness z_0 inside the diode, the COD process can be triggered by heating this segment. In this case, the COD is realised due to the damage inside the laser while the output facet remains intact (which, was described, for example, in [14]). This behaviour is typical of lasers with optically strengthened facets.

Acknowledgements. This work was partially supported by the Educational-Scientific Complex of P.N. Lebedev Physics Institute.

References

1. Miftakhutdinov D.R., Bogatov A.P., Drakin A.E. *Kvantovaya Elektron.*, **40** (7), 583 (2010) [*Quantum Electron.*, **40** (7), 583 (2010)].
2. Brugger H., Epperlein P.W. *Appl. Phys. Lett.*, **56** (11), 1049 (1990).
3. Tang W.C., Rosen H.J., Vettiger P., Webb D.J. *Proc. SPIE Int. Soc. Opt. Eng.*, **1634**, 198 (1992).
4. Tomm J.W., Thamm E., Bärwolff A., Elsaesser T., Luft J., Baeumler M., Mueller S., Jantz W., Rechenberg I., Erbert G. *Appl. Phys. A*, **70** (4), 377 (2000).
5. Rinner F., Roga J., Kelemen M.T., Mikulla M., Weimann G., Tomm J.W., Thamm E., Poprawe R. *J. Appl. Phys.*, **93** (3), 1848 (2003).
6. Tomm J.W., Esquivias I. *'Mirror Heating and COD in High-power Lasers (Catastrophic Optical Damage)', Tutorial at the BRIGHTER Meeting* (Lund University, Sweden, 2007).
7. Akimova I.V., Bogatov A.P., Drakin A.E., Konyaev V.P. *Kvantovaya Elektron.*, **25** (7), 647 (1998) [*Quantum Electron.*, **28** (7), 629 (1998)].
8. Miftakhutdinov D.R., D'yachkov N.V., Popovichev V.V., Nekrasov A.P., Drakin A.E., Bogatov A.P. *VI Belorussko-russkii seminar 'Poluprovodnikovye lazery i sistemy na ikh osnove'* (VI Belarusian-Russian Workshop 'Semiconductor Lasers and Systems Based on Them') (Minsk, 2007) p. 23.
9. Miftakhutdinov D.R., Akimova I.V., Bogatov A.P., Gushchik T.I., Drakin A.E., D'yachkov N.V., Popovichev V.V., Nekrasov A.P. *Kvantovaya Elektron.*, **38** (11), 993 (2008) [*Quantum Electron.*, **38** (11), 993 (2008)].
10. Horie H., Arai N., Mitsuishi Y., Komuro N., Kaneda H., Gotoh H., Usami M., Matsushima Y. *IEEE Photon. Techn. Lett.*, **12** (10), 1304 (2000).
11. Ressel P., Erbert G., Zeimer U., Hausler K., Beister G., Sumpf B., Klehr A., Trankle G. *IEEE Photon. Techn. Lett.*, **17** (5), 962 (2005).
12. Kamikawa T., Kawaguchi Y., Vaccaro P.O., Ito S., Kawanishi H. *Appl. Phys. Lett.*, **95** (3), 031106 (2009).
13. Fukuda M., Okayasu M., Temmyo J., Nakano J. *IEEE J. Quantum Electron.*, **30** (2), 471 (1994).
14. Chu S.N.G., Nakahara S., Twigg M.E., Koszi L.A., Plinn E.J., Chin A.K., Segner B.P., Johnston W.D. *J. Appl. Phys.*, **63** (3), 611 (1988).